Archives of Biochemistry and Biophysics 756 (2024) 109997

Contents lists available at ScienceDirect

Archives of Biochemistry and Biophysics

journal homepage: www.elsevier.com/locate/yabbi

A new preparation method of covalent annular nanodiscs based on MTGase

Yingkui Dong [a,b], Ming Li [b,c], Li Kang [a,b], Wanxue Wang [b,d], Zehua Li [b,c], Yizhuo Wang [b,c], Ziwei Wu [b,c], Chenchen Zhu [b,c], Lei Zhu [b], Xinwei Zheng [b], Dongming Qian [e], Han Dai [b,e], Bo Wu [b,***], Hongxin Zhao [b,e,*], Junfeng Wang [a,b,c,**]

[a] Institute of Physical Science and Information Technology, Anhui University, Hefei, Anhui, 230039, China
[b] High Magnetic Field Laboratory, Key Laboratory of High Magnetic Field and Ion Beam Physical Biology, Hefei Institutes of Physical Science, Chinese Academy of Sciences, Hefei, Anhui, 230031, China
[c] University of Science and Technology of China, Hefei, Anhui, 230026, China
[d] School of Basic Medical Sciences, Anhui Medical University, Hefei, Anhui, 230032, China
[e] Hefei China Science Longwood Biological Technology Co., Ltd. Hefei, Anhui, 230088, China

ARTICLE INFO

Keywords:
Nanodiscs
Microbial transglutaminases
Covalent annular nanodiscs
Membrane scaffold proteins

ABSTRACT

The preservation of the native conformation and functionality of membrane proteins has posed considerable challenges. While detergents and liposome reconstitution have been traditional approaches, nanodiscs (NDs) offer a promising solution by embedding membrane proteins in phospholipids encircled by an amphipathic helical protein MSP belt. Nevertheless, a drawback of commonly used NDs is their limited homogeneity and stability. In this study, we present a novel approach to construct covalent annular nanodiscs (cNDs) by leveraging microbial transglutaminase (MTGase) to catalyze isopeptide bond formation between the side chains of terminal amino acids, specifically Lysine (K) and Glutamine (Q). This methodology significantly enhances the homogeneity and stability of NDs. Characterization of cNDs and the assembly of membrane proteins within them validate the successful reconstitution of membrane proteins with improved homogeneity and stability. Our findings suggest that cNDs represent a more suitable tool for investigating interactions between membrane proteins and lipids, as well as for analyzing membrane protein structures.

1. Introduction

The term “biological membrane” (Biomembrane) encompasses all membrane structures found in biological cells [1]. These membranes, characterized by a phospholipid bilayer structure, fulfill vital functions of sealing and separating [2,3]. Serving as a selective permeability barrier, the main constituents of biological membranes are lipids and proteins. Within the bilayer structure, a multitude of lipid molecules align, creating a hydrophobic environment crucial for executing the functions of biological membranes [4]. This environment not only facilitates the correct folding and functioning of membrane proteins but also enables interactions between membrane proteins and lipids [4–7]. Biomembranes play a pivotal role in various essential biological activities within organisms. These activities include material transport, signal transduction, and significant physiological and biochemical processes, all of which necessitate the unique environment provided by biomembranes [8,9]. Consequently, the development of innovative biomembrane-like simulation systems becomes crucial for advancing membrane-related research.

Currently, there are four primary types of biomembrane-like simulation systems in use: Micelle, Bicelle, Liposome, and Nanodiscs [10]. Among these, Micelle stands as the most classic system, but its lack of a phospholipid membrane environment may lead to the denaturation of certain membrane proteins [11]. Liposome and Bicelle systems, though commonly employed in membrane-related research, pose challenges such as larger molecular weight, poor uniformity, and instability [12–16]. Nanodiscs (NDs), pioneered by Stephen Sligar’s group in 2002, represent a significant advancement [17]. Nanodiscs are disc-shaped

* Corresponding author. Hefei China Science Longwood Biological Technology Co., Ltd. Hefei, Anhui, 230088, China.
** Corresponding author. High Magnetic Field Laboratory, Key Laboratory of High Magnetic Field and Ion Beam Physical Biology, Hefei Institutes of Physical Science, Chinese Academy of Sciences, Hefei, Anhui, 230031, China
*** Corresponding author.
E-mail addresses: wubo@hmfl.ac.cn (B. Wu), zhx@hmfl.ac.cn (H. Zhao), junfeng@hmfl.ac.cn (J. Wang).

https://doi.org/10.1016/j.abb.2024.109997
Received 4 December 2023; Received in revised form 11 March 2024; Accepted 12 April 2024
Available online 16 April 2024

nanoparticles composed of a flat lipid bilayer surrounded by an amphiphilic molecular belt. To date, various types of amphiphilic belts, such as membrane scaffold proteins (MSPs) [18], peptides [19–21] and synthetic polymers [22–25], have been utilized for nanodisc assembly. Each type of belt offers distinct advantages but also has certain limitations, including interference with spectral absorbance [26–28] and non-specific interactions with target membrane proteins [29,30]. The recently developed non-ionic inulin polymers effectively eliminate any non-specific electrostatic interactions with target membrane proteins, making them highly suitable for investigating differently charged membrane proteins and protein complexes [31–33]. Traditional nanodiscs, known as MSP-nanodiscs, are formed through the self-assembly of linear MSPs [34]. MSP-nanodiscs present notable advantages in biomembrane research and find widespread application in studying the interactions between membrane proteins and lipids, analyzing membrane protein structures, researching vesicle transport and fusion, and facilitating targeted delivery of hydrophobic drugs [29,35–37]. However, challenges arise in studies utilizing nanodiscs assembled from linear MSPs, including issues with stability and uniformity due to size heterogeneity [38]. This may stem from the linear MSPs lacking a head-to-tail connection to form a closed-loop structure [38,39].

To address issues related to stability, size homogeneity, and tunability encountered with MSP-nanodiscs, researchers have introduced covalent annular nanodiscs (cNDs). The concept of cyclization for nanodiscs was initially proposed by Gerhard Wagner et al. [40], who successfully engineered Sortase-based cNDs. These cNDs boast advantages such as enhanced stability, a well-defined diameter size, and tunable shapes compared to traditional nanodiscs. In their work, Wagner and colleagues employed cNDs to co-assemble two membrane proteins, VDAC1 and NTR1, characterizing them through techniques such as nuclear magnetic resonance (NMR) and electron microscopy (EM). Additionally, cNDs have been instrumental in investigating the mechanism by which simple non-enveloped viruses transfer their genome across membranes to initiate infection. Subsequent advancements in cNDs development involved two distinct methodologies for self-cyclization, both leading to spontaneously generated cyclic products after expression [41,42]. One approach utilized intein-mediated ligation to achieve head-to-tail circularization, introducing a moderate ligation scar [41]. These cNDs, constructed using this method, prove suitable for EM and high-resolution NMR spectroscopy, making them versatile for a wide range of biophysical and biochemical applications. The second method applied SpyTag technology to produce a head-side chain cyclization product, resulting in a product carrying an insertion of approximately 120 amino acids [42]. This methodology found application in fusion pore reconstruction and protein-lipid interaction characterization. Collectively, these studies underscore the notable benefits of cNDs in addressing specific challenges associated with biomembrane-related investigations.

In this study, we have introduced a novel approach to produce cNDs through the catalytic formation mediated by Microbial transglutaminase (MTGase, EC: 2.3.2.13) [43]. Two short peptide sequences for MTGase reaction were strategically incorporated at both ends of MSP1D1, followed by the addition of MTGase for circularization. The results unequivocally demonstrate the successful generation of cNDs. Comprehensive characterizations of the constructed cNDs revealed favorable uniformity and stability. Leveraging MTGase-catalyzed cNDs, we proceeded to assemble the membrane protein VDAC1. The subsequent negative staining electron microscopy showcased the efficacy of the generated cNDs in successfully assembling membrane protein.

2. Materials and methods

2.1. Chemicals and reagents

Unless specifically stated, buffer components were from BBI (Sangon Biotech (Shanghai) Co., Ltd., China). All buffers were prepared with Milli-Q water (Merck/Millipore, Darmstadt, Germany). 1-Palmitoyl-2-oleoyl-*sn-glycero*-3-phosphocholine (POPC) and 1-Palmitoyl-2-oleoyl-*sn-glycero*-3-phosphatidylglycerol (POPG) were from Avanti Polar Lipids. LB medium components, (yeast extract and tryptone), were from ThermoFisher. MTGase was purchased from Yiming Biotechnology Company (100 U/g, Tai Xing City, Jiang Su province, China).

2.2. Plasmids

The plasmid containing the kqMSP1D1 and VDAC1 genes were custom-synthesized and codon-optimized by Beijing Tsingke Biotech Co., Ltd., China and inserted into the pET-28a (+) and pET-21b (+) vector. The protein sequences are:

kqMSP1D1

MHHHHHHHDY-
DIPTTENLYFQGKKGSGSGSSTFSKLREQLGPVTQEFWDNLEKE-
TEGLRQEMSKDLEEVKAKVQPYLDDFQKKWQEEME-
LYRQKVEPLRAELQEGARQKLHELQEKLSPLGEEMRDRAR-
AHVDALRTHLAPYSDELRQRLAARLEALKENGGARLAEYHAKA-
TEHLSTLSEKAKPALEDLRQGLLPVLESFKVSFLSA-
LEEYTKKLNTQGGGGSGGGGSLLQS*

VDAC1

MAVPPTYADLGKSARDVFTKGYGFGLIKLDLKTKSEN-
GLEFTSSGSANTETTKVTGSLETKYRWTEYGLTFTEKWNTDNTLGTEIT-
VEDQLARGLKLTFDSSFSPNTGKKNAKIKTGYKREHINLGCDMDFDIAG-
PSIRGALVLGYEGWLAGYQMNFE-
TAKSRVTQSNFAVGYKTDEFQLHTNVNDGTEFGGSIYQKVNKKLE-
TAVNLAWTAGNSNTRFGIAAKY-
QIDPDACFSAKVNNSSLIGLGYTQTLKPGIKLTLSALLDGKNV-
NAGGHKLGLGLEFQALEHHHHHH*

2.3. Expression and purification of kqMSP1D1 and VDAC1

Plasmid were transformed into *E. coli* BL21 (DE3). For protein expression, bacteria were grown in LB medium at 37 °C at 600 nm (OD600) of 0.8 and induced with 1 mM IPTG. After 4 h, the culture was centrifuged at 8000 rpm, 4 °C for 5 min. The bacterial pellet was resuspended with buffer A (50 mM Tris-HCl, 300 mM NaCl, 0.5 mM EDTA, pH 8.0), and disrupted with a pressure crusher at 600 ba. The lysate was centrifuged at 14000 rpm, 4 °C for 40 min. The supernatants were loaded onto a 5 ml Ni^{2+}-NTA column (GE Healthcare), followed by extensive wash (10 column volume, CV) using buffer A+ 1 % TritonX-100, buffer A + 50 mM Cholate, buffer A, buffer A + 20 mM imidazole and buffer A + 50 mM imidazole. Proteins were eluted with 5 CV of buffer A + 500 mM imidazole. The purity of the protein was checked by SDS-PAGE. The eluent was dialyzed in buffer B (20 mM Tris-HCl, 100 mM NaCl, 0.5 mM EDTA, pH 7.4) using an 8 kD MWCO membrane. 2 mM DTT and TEV protease (His 6 tagged; produced in-house) was added to the dialysate and incubated overnight at 4 °C. TEV was added at a ratio of protease to kqMSP1D1 protein of 1:100 (w/w). SDS-PAGE was performed to confirm that the N-terminal His tag is cleaved. After the TEV enzyme digestion was completed, the protein was concentrated to 300–500 μM, quick-frozen in liquid nitrogen, and stored at −80 °C.

The expression and purification method of VDAC1 is referred to previous reports [51].

2.4. Assemble of empty kqNDs and ckqNDs, as well as VDAC1-embedded ckqNDs

80 mM POPC: POPG = 3:2 lipid film was prepared. The corresponding mass of lipid was weighed, dissolved with chloroform, and blow dried with nitrogen, so that the lipid film evenly covers the inner

wall of the round bottom bottle, and was placed in a lyophilizer for lyophilization overnight. The lipid film was dissolved in 160 mM sodium cholate, aliquoted, frozen in liquid nitrogen, and store at −80 °C.

The mixture of MSPs and lipid with 1:65 M ratio were added into 1.5 ml Ep tube, hydrated with buffer B supplement to 500 μl (At this time, the kqMSP1D1 concentration is 0.2 mM), and incubated at 4 °C for 1 h. Then 0.2 g Biobeads SM-2 was added and incubated at 4 °C for 4 h to remove sodium cholate. After incubation, Biobeads was removed by filtration. For kqNDs assemble, the reaction mixture was purified on a Superdex 200 Increase 10/300 GL column. For ckqNDs assemble, MTGase was added to the reaction mixture with the final concentration of 0.175 U/mL, with buffer B supplement to 1 mL, and then incubated at 4 °C for 0.5 h to form ckqNDs, followed by purification through SEC on a Superdex 200 Increase 10/300 GL column.

To assemble VDAC1 into ckqNDs, 500 μL of 0.1 mM purified empty POPC-ckqNDs and 500 μL of 0.02 mM VDAC1 in LDAO detergent micelles were mixed at a molar ratio of 5:1 (ckqNDs:VDAC1), and incubated for 1 h at 4 °C. Subsequently, Biobeads SM-2 (0.5 g) were added and the mixture was further incubated for over 4 h at 4 °C. The removal of Bio-beads was achieved by passing through a gravity column with a volume of 3 mL. Separation between empty ckqNDs and ckqNDs containing VDAC1 was accomplished using Ni^{2+}-NTA affinity chromatography. The resulting reaction mixture was then subjected to purification on a Superdex 200 Increase 10/300 GL column equilibrated with buffer B, followed by collection of peak fractions for analysis via SDS-PAGE.

2.5. Mass spectrometry

The SDS-PAGE gel of target band was cut into 1 mm^3 cubes after being treated with acetonitrile, enzyme digestion solution was added for enzymatic digestion. Then extraction solution (5 % TFA-50 % ACN-45 % ddH2O) was added and incubated for 1 h at 37 °C water bath, sonicated for 5 min, centrifuged for 5 min. The extraction process was repeated once. The extracted peptides was lyophilized to near dryness and resuspend in 10 μL of 0.1 % formic acid before LC-MS/MS analysis.

NanoLC was performed using Nanoflow UPLC: Easy-nLC 1200 system (ThermoFisher Scientific, USA); and Nanocolumn:150 μm × 15 cm in-house made column packed with Acclaim PepMap RPLC C18 (1.9 μm, 100 Å, Dr. Maisch GmbH, Germany). Mass Spectrometry was performed using Q Exactive™ Hybrid Quadrupole-Orbitrap™ Mass Spectrometer (Thermo Fisher Scientific, USA).

The raw MS files were analyzed and searched against target protein database based on the species of the samples using Byonic. The parameters were set as follows: the protein modifications were carbamidomethylation (C) (fixed), oxidation (M) (variable), Acetyl (Protein N-term)(variable), K-1(+329.16)(K)(variable), K-2(+216.07)(K) (variable), the enzyme specificity was set to chymotrypsin; the maximum missed cleavages were set to 3; the precursor ion mass tolerance was set to 20 ppm, and MS/MS tolerance was 0.02 Da.

2.6. Negative stain electron microscopy

kqNDs (0.2 μM) and ckqNDs (0.2 μM) were applied onto freshly glow-discharged carbon coated copper grids (Zhongke Microscope). The sample was allowed to adsorb on the grid for 30 s before, the excess buffer was blotted away with a Whatmann filter paper. For desalting, the grid was washed twice with ddH_2O before the sample was stained in freshly prepared 2 % uranyl acetate for 1 min, and air dried. The grids were imaged in a Tecnai G2 F20 (FEI) electron microscope operating at a voltage of 200 kV. For the details of particle diameter distribution and discoidal shape analysis, 2D class averaging was performed by selecting at least 4000 particles, with EMAN2 [52] picking and relion 3.1.3 [53] classification.

2.7. Dynamic light scattering

Dynamic light scattering (DLS) experiments were performed on a Malvern Zetasizer Nano ZS equipped with a He–Ne laser as the light source (wavelength: 633 nm; scattering angle: 173°) at 25 °C. The sample was diluted with a buffer B, and 1 mL of each sample was measured (11 runs of 10 s) in triplicate in a single-use disposable cuvette (Malvern, DTS0012) with a 10-mm path length. For the DLS variable temperature experiment, the temperature was programmed to ramp from 20 °C to 70 °C at a rate of 1 °C/min. Each temperature was maintained for 30 s, and the sample was measured in triplicate as described above. Data was analyzed using the Zetasizer Software 7.11 (Malvern Instruments Ltd., Malvern, UK).

2.8. Circular dichroism spectroscopy

Circular dichroism (CD) experiments were performed at room temperature from 190 to 260 nm with a Jasco J-1700 CD Spectrometer (Tokyo, Japan). Spectra were collected in quartz cuvettes with a 1 mm path length and averaged across three consecutive scans. A 0.5 nm data pitch and 1 nm bandwidth were generally used. Thermal melts were acquired by monitoring the change in the CD signal at 222 nm as a function of temperature, from 20 to 90 °C, 1 °C interval, and 10 °C/min gradient. The protein concentration was 10 μM in 20 mM potassium phosphate, pH 7.4. Spectra were corrected for buffer contributions.

2.9. Statistics

Origin 2022 is used to analyze data generated in the EM. Diameter measurements were done with ImageJ software.

3. Results

3.1. Design of kqMSP1D1 and construction of cNDs

MTGase demonstrates the capability to catalyze the acyl transfer reaction, specifically between the γ-carboxamide group of the glutamine residue (acyl donor) and the ε-amino group of the lysine residue (acyl acceptor). This enzymatic activity results in the formation of an ε-(γ-glutamine)-lysine isopeptide bond (Fig. 1A) [43]. To harness this catalytic potential, we introduced two short peptide sequences crucial for the reaction into the MSP1D1 sequence, to form kqMSP1D1. These sequences include the K donor dipeptide KK at the N terminus and the Q donor Q tag (with the amino acid sequence LLQS) at the C terminus. The incorporation was achieved through GS linkers, creating a fusion protein denoted as kqMSP1D1 (Fig. 1B) [44]. This strategic design aims to facilitate the MTGase-catalyzed circularization process, forming a covalent annular kqNanodiscs structure, ckqNDs.

The designed kqMSP1D1 sequence was expressed in *Escherichia coli* BL21 (DE3) and subsequently purified. Notably, the results of the expression and purification processes revealed that the constructed kqMSP1D1 proteins were soluble. The purified kqMSP1D1 protein exhibited a yield of approximately 20 mg/L, slightly lower than that of MSP1D1 (around 25 mg/L) [45]. With the obtained kqMSP1D1 protein, we initially explored traditional non-covalent assembly to assess its potential to form kqNanodiscs (kqNDs). The successful formation of kqNDs was confirmed through Size Exclusion Chromatography (SEC). As shown in Fig. S1, kqNDs have an elution volume of 12.5 ml, which is the same as that of the NDs prepared with MSP1D1. Building upon this traditional non-covalent nanodisc formation, we introduced MTGase for the acyl transfer reaction, allowing it to proceed for 0.5 h. The resulting reaction mixture underwent purification by SEC, we obtained the MTGase-treated particles (Fig. 1C and Fig. S2).

To assess the differences between the constructed kqNDs and MTGase-treated particles, we conducted a comparison utilizing SEC. The elution volumes for kqNDs and MTGase-treated particles were

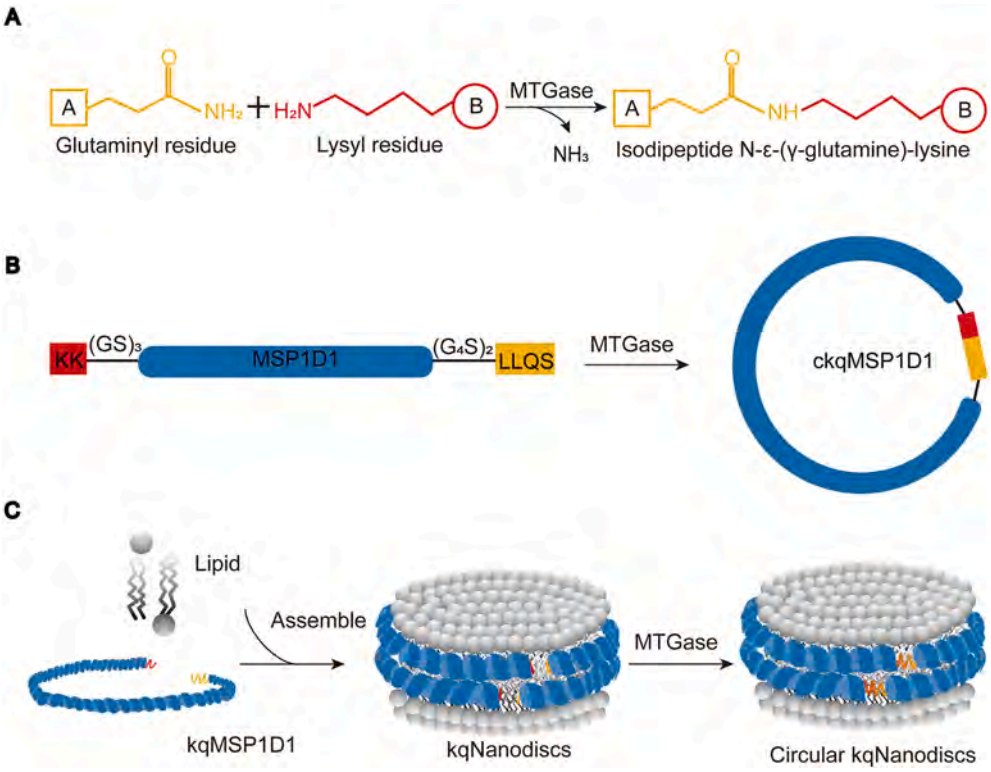

Fig. 1. Mechanism of MTGase-Catalyzed Protein Ligation A) Principle of MTGase-Catalyzed Protein Ligation: Illustration depicting the fundamental concept behind catalyzing protein ligation using MTGase. B) Design of kqMSP1D1 and Schematic Circularization of ckqMSP1D1: Design details of kqMSP1D1, including a schematic representation of the circularization process for ckqMSP1D1. C) Assembly Process of ckqNDs: Visualization of the stepwise assembly process leading to ckqNDs formation.

determined to be 12.5 ml and 12.1 ml, respectively. The SEC chromatogram (Fig. 2A) revealed a distinct shift, with the peak of MTGase-treated particles eluting slightly earlier compared to that of kqNDs. Further analysis through SDS-PAGE corroborated these findings. Notably, the bands corresponding to MTGase-treated particles exhibited a downward shift compared to the bands of kqNDs, possibly due to its more compact conformation. (Fig. 2B). Intriguingly, a similar phenomenon has been observed in other studies utilizing various methods such as Sortase, Split-Intein, SpyCatcher/SpyTag, etc [40–42].

3.2. Determination of cyclization linkage in MTGase-treated particles

To validate the covalent cyclization of MTGase-treated particles, the SDS-PAGE band of the particles (Fig. 2B, lane 3) was subjected to chymotrypsin digestion and subsequently analyzed using liquid chromatography-tandem mass spectrometry (LC-MS/MS). We selected chymotrypsin for enzymatic digestion due to its preference for cleaving protein chains at the carboxyl side of aromatic amino acids and Leu, enabling us to identify peptides with cyclization sites. During the analysis, our focus was on identifying the peptide that forms a linkage between the N and C terminus residues of kqMSP1D1, catalyzed by MTGase. The outcomes of this investigation pointed specifically to the kqMSP1D1 protein we constructed. The expected cleavage points with chymotrypsin and the putative linked and unlinked peptides are shown in Fig. S3. Consequently, two chymotryptic peptide precursor ions were successfully identified with m/z values of 658.32 (Fig. 2C) and 439.21 (Fig. S4). Both ions matched peptide 1 (Fig. S3), and this was further confirmed by their MS/MS fragmentation spectrum. The LC-M/MS results clearly demonstrated a noteworthy observation: only the side chain group of K at the N terminus underwent a transamination reaction with Q in the Q-tag at the C terminus. This interaction culminated in the formation of an ε (γ-glutamyl) lysine bridge, affirming the successful construction of ckqNDs with covalently linked head and tail side chains.

3.3. Biophysical Characterization of kqNDs and ckqNDs

Dynamic light scattering (DLS) experiments were conducted to precisely measure the particle sizes of kqNDs and ckqNDs in solution. The DLS data revealed that the particle size of ckqNDs was 12.3 ± 3.6 nm, slightly larger than that of kqNDs, which measured 11.3 ± 3.8 nm (Fig. 3A). To further confirm the formation and assess the size of the nanodiscs, negative staining electron microscopy was employed for detailed observation (Fig. 3B (a) and (c)). The constructed ckqNDs exhibited an appearance similar to that of kqNDs, consistent with the expected morphology of nanodiscs. Diameters were measured, and statistical analysis of size distribution (Fig. 3B (b) and (d)) indicated that the average diameter of ckqNDs was approximately 11.7 ± 2.5 nm, slightly larger than that of kqNDs, which measured 10.7 ± 2.8 nm. It's noteworthy that the DLS results appeared larger than those obtained from negative stain electron microscopy. This discrepancy can be attributed to the fact that the measured hydrated particle size of nanodiscs in the solution tends to be larger [46]. These combined results from DLS and negative stain transmission electron microscopy affirm that the constructed ckqNDs exhibit excellent uniformity.

To evaluate the stability of the secondary structure of MSP1D1, we conducted circular dichroism spectroscopy (CD) comparisons among kqMSP1D1, POPC-based kqNDs and ckqNDs. The resulting CD spectra (Fig. 3C) unequivocally confirmed the helical nature of all samples in solution, characterized by distinctive minima at 208 and 222 nm, indicative of helical structures. Notably, when contrasting the phospholipid-free MSP1D1 sample with the nanodisc samples, a noteworthy increase in the CD signal at 222 nm was observed for the nanodiscs. This observation is consistent with the well-established fact that the helicity of MSPs increases when nanodiscs are formed [17,47,

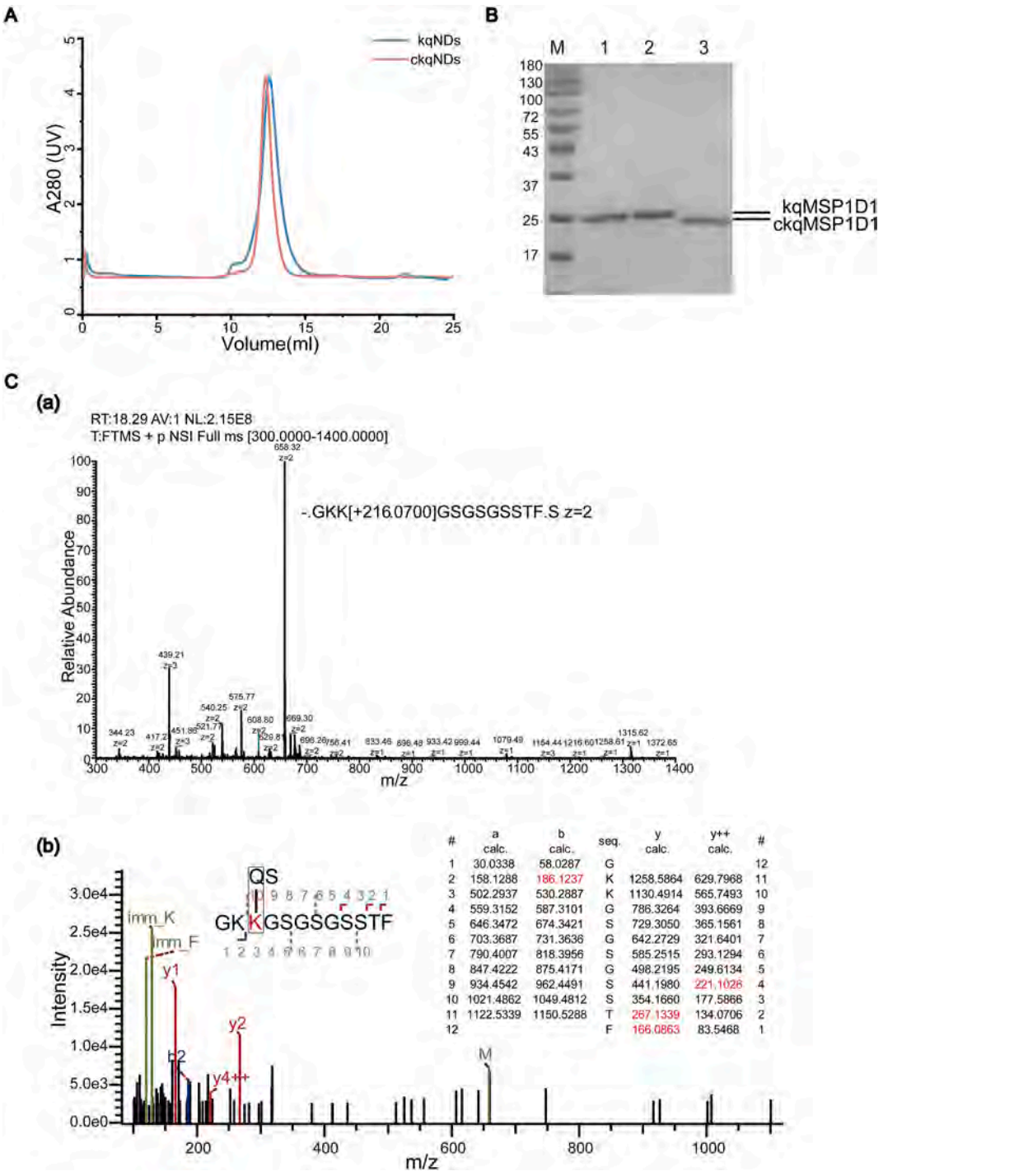

Fig. 2. Determination of ckqNDs Linkage by LC-MS/MS A) Comparison of SEC chromatograms between kqNDs and ckqNDs. B) SDS-PAGE of NDs. (M: marker, 1: kqMSP1D1, 2: kqNDs, 3: ckqNDs.) C) (a) The precursor ion of a chymotryptic peptide with *m/z* value of 658.32 and z = 2. (b) MS/MS fragmentation spectrum of this chymotryptic peptide.

48].

To assess the stability of kqNDs and ckqNDs, we initially performed thermal melting experiments by monitoring the CD signal at λ = 222 nm (Fig. S5). The results demonstrate that the thermal stability of ckqMSP belt within nanodiscs is comparable to that of kqMSP belt, with respective melting temperature (Tm) values of 78.1 °C and 80.4 °C. This finding aligns with a recent study reporting similar thermal stability between cyclization MSP1D1 generated through a split-intein-based approach and its linear form in nanodiscs [41]. To better evaluate the thermal stability of intact kqNDs and ckqNDs, we conducted variable temperature DLS experiments. As shown in Fig. 3D, the average diameter of kqNDs remained relatively stable below 50 °C, but experienced a significant increase from 50 to 70 °C, reaching a value of 55.2 nm. Conversely, the average diameter of ckqNDs exhibited stability below 57 °C and gradually increased to 22.6 nm as the temperature rose from 57 to 70 °C. These findings demonstrate that kqNDs cross-linked using MTGase exhibit superior thermal stability compared to their non-cross-linked counterparts.

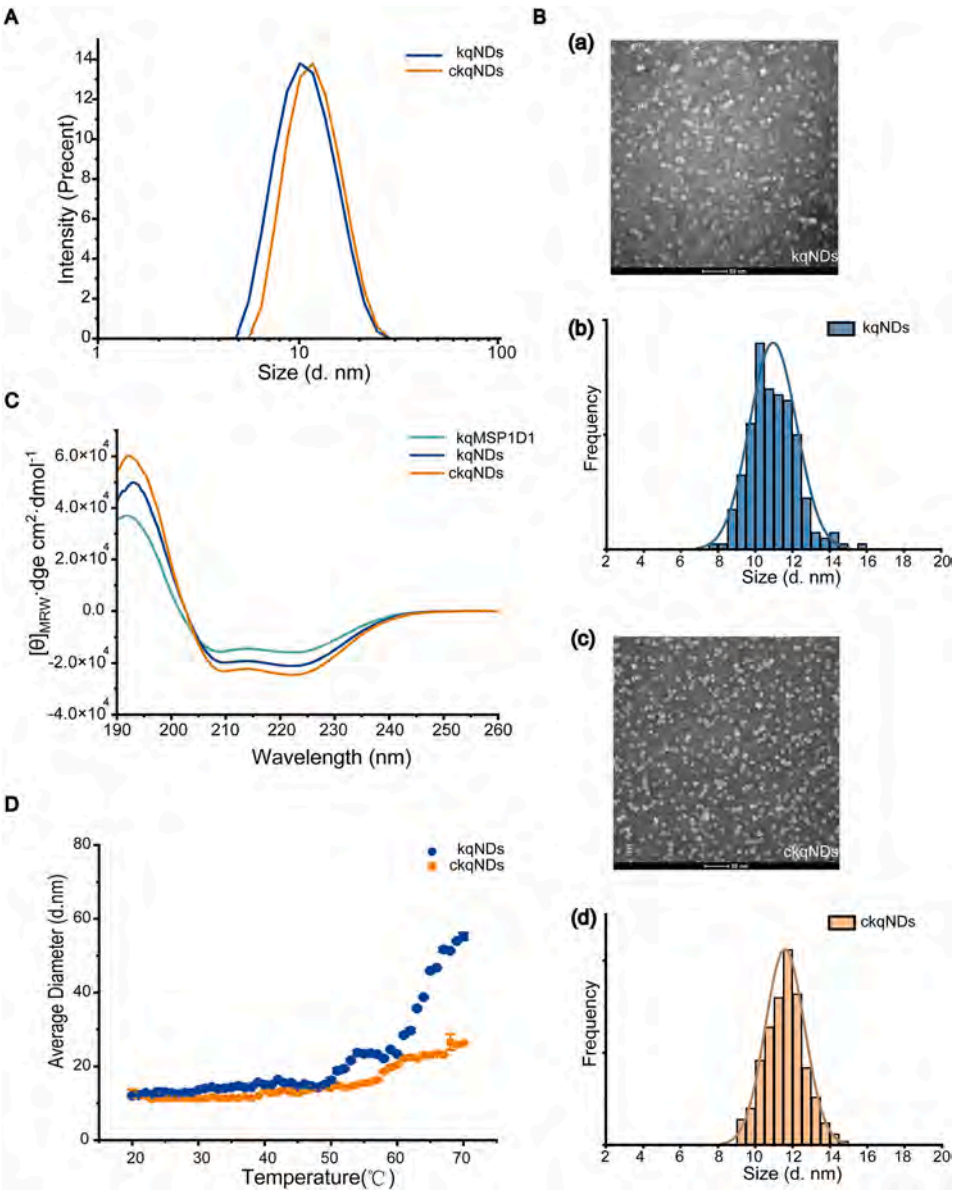

Fig. 3. Biophysical Characterization of ckqNDs A) DLS analysis of particle size for kqNDs and ckqNDs. (ckqNDs: 12.3 ± 3.6 nm, kqNDs: 11.3 ± 3.8 nm) B) (a) Negative staining electron microscopy observation and (b) Particle size statistical distribution analysis of kqNDs, with a statistical result of 10.7 ± 2.8 nm. (c) Negative staining electron microscopy observation and (d) particle size statistical distribution analysis of ckqNDs, with a statistical result of 11.7 ± 2.8 nm. C) Near-UV CD spectroscopy of kqMSP1D1, kqNDs, and ckqNDs. D) Thermal unfolding of kqNDs and ckqNDs monitored by DLS.

3.4. Assembly of VDAC1 in ckqNDs

The assembly of human Voltage-Dependent Anion Channel subtype 1 (VDAC1, 32 kDa) in ckqNDs was achieved through a meticulous process. Initially, ckqNDs were purified following the previously outlined method. Subsequently, the membrane protein VDAC1 was co-incubated with the detergent mixture within the constructed ckqNDs. Bio-beads were introduced to eliminate the detergent, and the assembled VDAC1 protein within ckqNDs was purified and isolated using SEC purification (Fig. 4A and B). The confirmation of VDAC1 assembly within ckqNDs was established through negative staining electron microscopy, revealing not only successful assembly but also demonstrating good uniformity (Fig. 4C (a) and (b)). Further support for the assembly was obtained through the analysis of 2D class averages (Fig. 4C (c)), confirming the successful incorporation of VDAC1 into ckqNDs. This substantiates that the covalent annular nanodiscs we constructed serve as an effective tool for the study of membrane proteins.

4. Discussion

This study introduces a streamlined and efficient approach for the rapid preparation of cNDs. The constructed ckqNDs exhibit a straightforward implementation process. The soluble expressed kqMSP1D1 facilitates the ease of subsequent experiments, contributing to the overall feasibility of the method. Furthermore, the method leverages the cost-effective and readily available MTGase. Its high catalytic reaction rate not only ensures efficiency but also proves advantageous in terms of time and cost savings. This innovative method not only simplifies the preparation of cNDs but also enhances the accessibility and practicality of utilizing this novel nanodiscs system in diverse experimental contexts.

The cNDs meticulously developed in this study showcase remarkable uniformity and thermal stability. Examination of ckqNDs through negative stain electron microscopy reveals structural characteristics consistent with the anticipated features of nanodiscs. The measured size of the ckqNDs, approximately 11.7 ± 2.5 nm, closely aligns with the

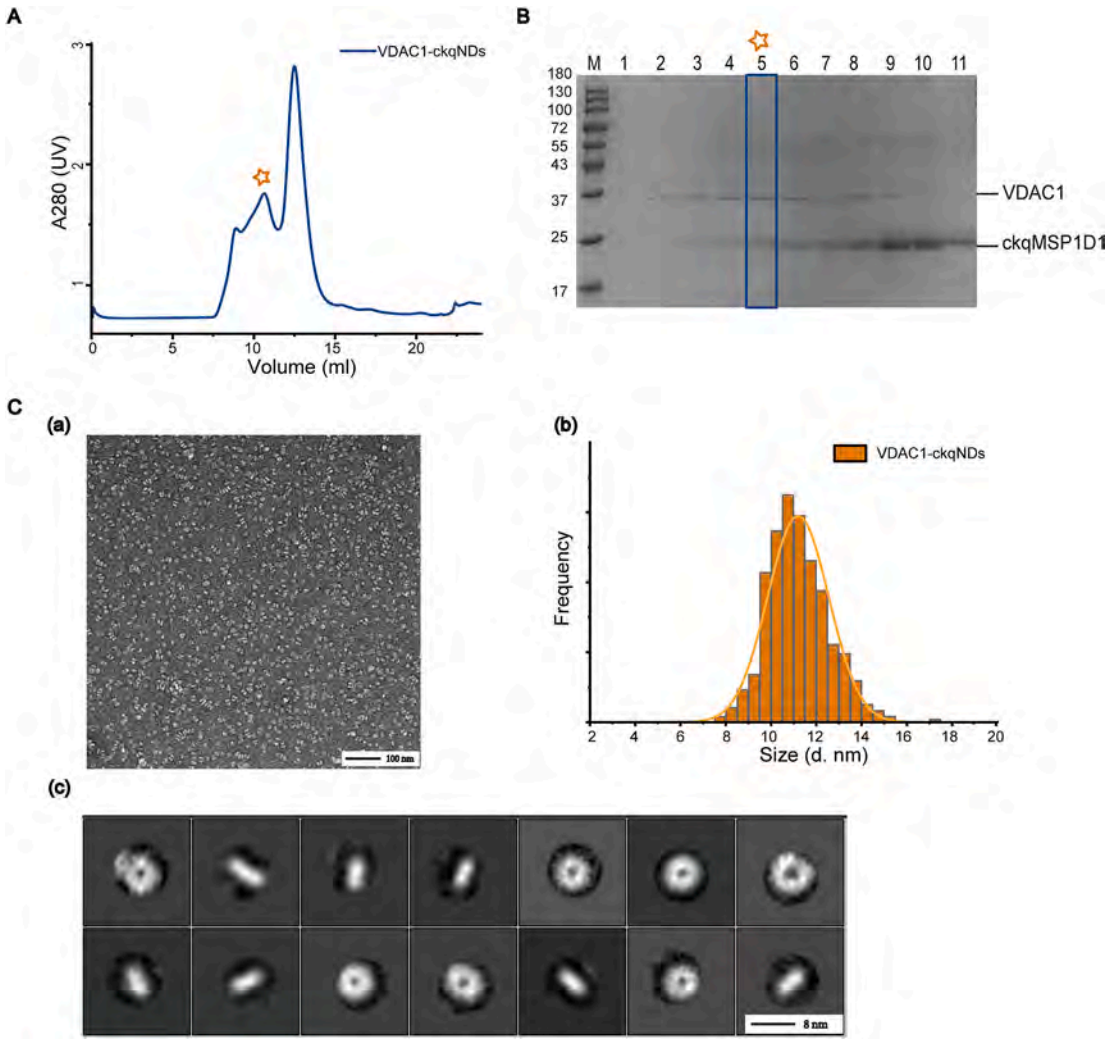

Fig. 4. Assembly of VDAC1 in ckqNDs A) SEC profile of VDAC1 assembly in ckqNDs. B) SDS-PAGE of SEC fractions. C) (a) Negative stain electron microscopy of assembled VDAC1-ckqNDs. The collected protein corresponding to sample No. 5 was selected for visualization. (b) Particle size statistical distribution analysis of VDAC1-ckqNDs. (c) Counterstain electron microscopy of VDAC1-ckqNDs for 2D class average. The VDAC1 protein appears as dark spots inside the nanodisc.

dimensions reported for cMSP1D1 nanodiscs produced using methodologies such as Sortase, Split-Intein, SpyCatcher/SpyTag, etc. [40–42]. In thermal unfolding experiments, a qualitative assessment demonstrates an augmented thermal stability in the ckqNDs. These findings harmonize with broader observations concerning cNDs generated through alternative methodologies [48–50]. Moreover, the versatility of the constructed ckqNDs is highlighted by their ability to effectively assemble VDAC1, a model protein. This successful protein assembly underscores the functional integrity of the ckqNDs in facilitating the incorporation of membrane proteins. It should be noted that the broad substrate specificity of MTGase has the potential to result in cross-linking of target membrane proteins during their incorporation into ckqNDs if MTGase is present. However, this issue can be effectively circumvented by initially obtaining purified empty ckqNDs and subsequently assembling the target membrane protein without the presence of MTGase, as demonstrated in our VDAC1 assembly process.

In summary, our study introduces a rapid and cost-effective method for the generation of cNDs. This novel approach holds significant promise for advancing research in the exploration of interactions between membrane proteins and lipids, as well as the elucidation of membrane protein structures in future studies.

Conflicts of interest

The authors declare that they have no conflict of interest.

Funding information

We thank this work was supported by funds from, Anhui Major Basic Research Projects (grant no. 2023z04020016 to JW), the National Natural Science Foundation of China (grant no. 32371362 to BW and 32171226 to LZ), and the Hefei Institutes of Physical Science Director's Fund (grant no. BJPY2022B08 to LZ and YZJJZX202014 to JW).

CRediT authorship contribution statement

Yingkui Dong: Writing – original draft, Validation, Methodology, Investigation, Conceptualization. **Ming Li:** Resources, Investigation. **Li Kang:** Validation. **Wanxue Wang:** Validation. **Zehua Li:** Resources. **Yizhuo Wang:** Resources. **Ziwei Wu:** Resources. **Chenchen Zhu:** Resources. **Lei Zhu:** Funding acquisition. **Xinwei Zheng:** Resources. **Dongming Qian:** Resources. **Han Dai:** Writing – original draft. **Bo Wu:** Supervision, Project administration, Writing – review & editing. **Hongxin Zhao:** Conceptualization, Methodology, Project administration. **Junfeng Wang:** Funding acquisition, Project administration, Supervision, Writing – review & editing.

Acknowledgements

We are grateful to mass spectrometry system at the High Magnetic Field Laboratory of the Chinese Academy of Sciences for instrument support and technical assistance.

Appendix A. Supplementary data

Supplementary data to this article can be found online at https://doi.org/10.1016/j.abb.2024.109997.

References

[1] Y.Y. Jiang, D.X. Kong, T. Qin, X. Li, G. Caetano-Anolles, H.Y. Zhang, The impact of oxygen on metabolic evolution: a chemoinformatic investigation, PLoS Comput. Biol. 8 (3) (2012) e1002426, https://doi.org/10.1371/journal.pcbi.1002426.
[2] A.J. Garcia-Saez, P. Schwille, Surface analysis of membrane dynamics, Biochim. Biophys. Acta 1798 (4) (2010) 766–776, https://doi.org/10.1016/j.bbamem.2009.09.016.
[3] M. Pasenkiewicz-Gierula, K. Murzyn, T. Rog, C. Czaplewski, Molecular dynamics simulation studies of lipid bilayer systems, Acta Biochim. Pol. 47 (3) (2000) 601–611.
[4] B. Krishnarjuna, A. Ramamoorthy, Detergent-free isolation of membrane proteins and strategies to study them in a near-native membrane environment, Biomolecules 12 (8) (2022), https://doi.org/10.3390/biom12081076.
[5] K. Abe, Y. Fujiyoshi, Cryo-electron microscopy for structure analyses of membrane proteins in the lipid bilayer, Curr. Opin. Struct. Biol. 39 (2016) 71–78, https://doi.org/10.1016/j.sbi.2016.06.001.
[6] A.L. Duncan, Monolysocardiolipin (MLCL) interactions with mitochondrial membrane proteins, Biochem. Soc. Trans. 48 (3) (2020) 993–1004, https://doi.org/10.1042/BST20190932.
[7] A.M. Whited, A. Johs, The interactions of peripheral membrane proteins with biological membranes, Chem. Phys. Lipids 192 (2015) 51–59, https://doi.org/10.1016/j.chemphyslip.2015.07.015.
[8] D. Marsh, L.I. Horvath, M.J. Swamy, S. Mantripragada, J.H. Kleinschmidt, Interaction of membrane-spanning proteins with peripheral and lipid-anchored membrane proteins: perspectives from protein-lipid interactions (Review), Mol. Membr. Biol. 19 (4) (2002) 247–255, https://doi.org/10.1080/09687680210162419.
[9] A. Barba-Bon, M. Nilam, A. Hennig, Supramolecular chemistry in the biomembrane, Chembiochem 21 (7) (2020) 886–910, https://doi.org/10.1002/cbic.201900646.
[10] E.J. Dufourc, Bicelles and nanodiscs for biophysical chemistry, Biochim. Biophys. Acta Biomembr. 1863 (1) (2021) 183478, https://doi.org/10.1016/j.bbamem.2020.183478.
[11] D. Milic, D.B. Veprintsev, Large-scale production and protein engineering of G protein-coupled receptors for structural studies, Front. Pharmacol. 6 (2015) 66, https://doi.org/10.3389/fphar.2015.00066.
[12] L. Barbosa-Barros, G. Rodriguez, C. Barba, M. Cocera, L. Rubio, J. Estelrich, C. Lopez-Iglesias, A. de la Maza, O. Lopez, Bicelles: lipid nanostructured platforms with potential dermal applications, Small 8 (6) (2012) 807–818, https://doi.org/10.1002/smll.201101545.
[13] L. Zou, Q. Li, Y. Hou, M. Chen, X. Xu, H. Wu, Z. Sun, G. Ma, Self-assembled glycyrrhetinic acid derivatives for functional applications: a review, Food Funct. 13 (24) (2022) 12487–12509, https://doi.org/10.1039/d2fo02472a.
[14] Z.W. Lu, W.D. Van Horn, J. Chen, S. Mathew, R. Zent, C.R. Sanders, Bicelles at low concentrations, Mol. Pharm. 9 (4) (2012) 752–761, https://doi.org/10.1021/mp2004687.
[15] U.H.N. Dürr, R. Soong, A. Ramamoorthy, When detergent meets bilayer: birth and coming of age of lipid bicelles, Prog. Nucl. Magn. Reson. Spectrosc. 69 (2013) 1–22, https://doi.org/10.1016/j.pnmrs.2013.01.001.
[16] U.H.N. Dürr, M. Gildenberg, A. Ramamoorthy, The magic of bicelles lights up membrane protein structure, Chem. Rev. 112 (11) (2012) 6054–6074, https://doi.org/10.1021/cr300061w.
[17] T.H. Bayburt, Y.V. Grinkova, S.G. Sligar, Self-assembly of discoidal phospholipid bilayer nanoparticles with membrane scaffold proteins, Nano Lett. 2 (8) (2002) 853–856, https://doi.org/10.1021/nl025623k.
[18] I.G. Denisov, Y.V. Grinkova, A.A. Lazarides, S.G. Sligar, Directed self-assembly of monodisperse phospholipid bilayer Nanodiscs with controlled size, J. Am. Chem. Soc. 126 (11) (2004) 3477–3487, https://doi.org/10.1021/ja0393574.
[19] D.C.R. Camargo, K.J. Korshavn, A. Jussupow, K. Raltchev, D. Goricanec, M. Fleisch, R. Sarkar, K. Xue, M. Aichler, G. Mettenleiter, A.K. Walch, C. Camilloni, F. Hagn, B. Reif, A. Ramamoorthy, Stabilization and structural analysis of a membrane-associated hIAPP aggregation intermediate, Elife 6 (2017), https://doi.org/10.7554/eLife.31226. ARTN e31226.
[20] C. Barnaba, B.R. Sahoo, T. Ravula, I.G. Medina-Meza, S.C. Im, G. M. Anantharamaiah, L. Waskell, A. Ramamoorthy, Cytochrome-P450-Induced ordering of microsomal membranes modulates affinity for drugs, Angew. Chem., Int. Ed. 57 (13) (2018) 3391–3395, https://doi.org/10.1002/anie.201713167.
[21] C. Barnaba, A. Ramamoorthy, Picturing the membrane-assisted choreography of cytochrome P450 with lipid nanodiscs, ChemPhysChem 19 (20) (2018) 2603–2613, https://doi.org/10.1002/cphc.201800444.
[22] R.C. Arenas, J. Klingler, C. Vargas, S. Keller, Influence of lipid bilayer properties on nanodisc formation mediated by styrene/maleic acid copolymers, Nanoscale 8 (32) (2016) 15016–15026, https://doi.org/10.1039/c6nr02089e.
[23] G.M. Di Mauro, C. La Rosa, M. Condorelli, A. Ramamoorthy, Benchmarks of SMA-copolymer derivatives and nanodisc integrity, Langmuir 37 (10) (2021) 3113–3121, https://doi.org/10.1021/acs.langmuir.0c03554.
[24] T. Ravula, N.Z. Hardin, S.K. Ramadugu, S.J. Cox, A. Ramamoorthy, Formation of pH-resistant monodispersed polymer-lipid bilayer nanodiscs (vol 57, pg 1342, 2018), Angew. Chem., Int. Ed. 58 (38) (2019), https://doi.org/10.1002/anie.201906504, 13185-13185.
[25] B.R. Sahoo, T. Genjo, M. Bekier, S.J. Cox, A.K. Stoddard, M. Ivanova, K. Yasuhara, C.A. Fierke, Y.Z. Wang, A. Ramamoorthy, Alzheimer's amyloid-beta intermediates generated using polymer-nanodiscs, Chem. Commun. 54 (91) (2018) 12883–12886, https://doi.org/10.1039/c8cc07921h.
[26] M. Zhang, R. Huang, R. Ackermann, S.C. Im, L. Waskell, A. Schwendeman, A. Ramamoorthy, Reconstitution of the Cyt-CytP450 complex in nanodiscs for structural studies using NMR spectroscopy, Angew. Chem., Int. Ed. 55 (14) (2016) 4497–4499, https://doi.org/10.1002/anie.201600073.
[27] E. Prade, M. Mahajan, S.C. Im, M. Zhang, K.A. Gentry, G.M. Anantharamaiah, L. Waskell, A. Ramamoorthy, A minimal functional complex of cytochrome P450 and FBD of cytochrome P450 reductase in nanodiscs, Angew. Chem., Int. Ed. 57 (28) (2018) 8458–8462, https://doi.org/10.1002/anie.201802210.
[28] T. Ravula, D. Ishikuro, N. Kodera, T. Ando, G.M. Anantharamaiah, A. Ramamoorthy, Real-time monitoring of lipid exchange via fusion of peptide based lipid-nanodiscs, Chem. Mater. 30 (10) (2018) 3204–3207, https://doi.org/10.1021/acs.chemmater.8b00946.
[29] T. Ravula, N.Z. Hardin, A. Ramamoorthy, Polymer nanodiscs: advantages and limitations, Chem. Phys. Lipids 219 (2019) 45–49, https://doi.org/10.1016/j.chemphyslip.2019.01.010.
[30] T. Ravula, N.Z. Hardin, J. Bai, S.C. Im, L. Waskell, A. Ramamoorthy, Effect of polymer charge on functional reconstitution of membrane proteins in polymer nanodiscs, Chem. Commun. 54 (69) (2018) 9615–9618, https://doi.org/10.1039/c8cc04184a.
[31] T. Ravula, A. Ramamoorthy, Synthesis, characterization, and nanodisc formation of non-ionic polymers, Angew. Chem., Int. Ed. 60 (31) (2021) 16885–16888, https://doi.org/10.1002/anie.202101950.
[32] B. Krishnarjuna, S.G. Im, T. Ravula, J. Marte, R.J. Auchus, A. Ramamoorthy, Non-ionic inulin-based polymer nanodiscs enable functional reconstitution of a redox complex composed of oppositely charged CYP450 and CPR in a lipid bilayer membrane, Anal. Chem. 94 (34) (2022) 11908–11915, https://doi.org/10.1021/acs.analchem.2c02489.
[33] B. Krishnarjuna, J. Marte, T. Ravula, A. Ramamoorthy, Enhancing the stability and homogeneity of non-ionic polymer nanodiscs by tuning electrostatic interactions, J. Colloid Interface Sci. 634 (2023) 887–896, https://doi.org/10.1016/j.jcis.2022.12.112.
[34] I.G. Denisov, S.G. Sligar, Nanodiscs in membrane biochemistry and biophysics, Chem. Rev. 117 (6) (2017) 4669–4713, https://doi.org/10.1021/acs.chemrev.6b00690.
[35] M.D. Farrelly, L.L. Martin, S.H. Thang, Polymer nanodiscs and their bioanalytical potential, Chem. Eur J. 27 (51) (2021) 12922–12939, https://doi.org/10.1002/chem.202101572.
[36] S.G. Sligar, I.G. Denisov, Nanodiscs: a toolkit for membrane protein science, Protein Sci. 30 (2) (2021) 297–315, https://doi.org/10.1002/pro.3994.
[37] I.G. Denisov, S.G. Sligar, Nanodiscs for structural and functional studies of membrane proteins, Nat. Struct. Mol. Biol. 23 (6) (2016) 481–486, https://doi.org/10.1038/nsmb.3195.
[38] M.L. Nasr, Large nanodiscs going viral, Curr. Opin. Struct. Biol. 60 (2020) 150–156, https://doi.org/10.1016/j.sbi.2020.01.006.
[39] M.L. Nasr, G. Wagner, Covalently circularized nanodiscs; challenges and applications, Curr. Opin. Struct. Biol. 51 (2018) 129–134, https://doi.org/10.1016/j.sbi.2018.03.014.
[40] M.L. Nasr, D. Baptista, M. Strauss, Z.J. Sun, S. Grigoriu, S. Huser, A. Pluckthun, F. Hagn, T. Walz, J.M. Hogle, G. Wagner, Covalently circularized nanodiscs for studying membrane proteins and viral entry, Nat. Methods 14 (1) (2017) 49–52, https://doi.org/10.1038/nmeth.4079.
[41] J. Miehling, D. Goricanec, F. Hagn, A split-intein-based method for the efficient production o f circularized nanodiscs for structural studies of membrane proteins, Chembiochem 19 (18) (2018) 1927–1933, https://doi.org/10.1002/cbic.201800345.
[42] S. Zhang, Q. Ren, S.J. Novick, T.S. Strutzenberg, P.R. Griffin, H. Bao, One-step construction of circularized nanodiscs using SpyCatcher-SpyTag, Nat. Commun. 12 (1) (2021) 5451, https://doi.org/10.1038/s41467-021-25737-7.
[43] Y. Anami, K. Tsuchikama, Transglutaminase-mediated conjugations, Methods Mol. Biol. 2078 (2020) 71–82, https://doi.org/10.1007/978-1-4939-9929-3_5.
[44] M. Liu, Y. Zhu, T. Wu, J. Cheng, Y. Liu, Nanobody-ferritin conjugate for targeted photodynamic therapy, Chemistry 26 (33) (2020) 7442–7450, https://doi.org/10.1002/chem.202000075.
[45] R. Puthenveetil, O. Vinogradova, Optimization of the design and preparation of nanoscale phospholipid bilayers for its application to solution NMR, Proteins 81 (7) (2013) 1222–1231, https://doi.org/10.1002/prot.24271.
[46] B. Lorber, F. Fischer, M. Bailly, H. Roy, D. Kern, Protein analysis by dynamic light scattering: methods and techniques for students, Biochem. Mol. Biol. Educ. 40 (6) (2012) 372–382, https://doi.org/10.1002/bmb.20644.
[47] Q. Ren, S. Zhang, H. Bao, Circularized fluorescent nanodiscs for probing protein-lipid interactions, Commun. Biol. 5 (1) (2022) 507, https://doi.org/10.1038/s42003-022-03443-4.

[48] N.T. Johansen, F.G. Tidemand, T. Nguyen, K.D. Rand, M.C. Pedersen, L. Arleth, Circularized and solubility-enhanced MSPs facilitate simple and high-yield production of stable nanodiscs for studies of membrane proteins in solution, FEBS J. 286 (9) (2019) 1734–1751, https://doi.org/10.1111/febs.14766.

[49] Y. Yusuf, J. Massiot, Y.T. Chang, P.H. Wu, V. Yeh, P.C. Kuo, J. Shiue, T.Y. Yu, Optimization of the production of covalently circularized nanodiscs and their characterization in physiological conditions, Langmuir 34 (11) (2018) 3525–3532, https://doi.org/10.1021/acs.langmuir.8b00025.

[50] X.Y. Jia, Y.K.Y. Chin, A.H. Zhang, T. Crawford, Y.F. Zhu, N.L. Fletcher, Z.H. Zhou, B.R. Hamilton, M. Stroet, K.J. Thurecht, M. Mobli, Self-cyclisation as a general and efficient platform for peptide and protein macrocyclisation, Commun. Chem. 6 (1) (2023), https://doi.org/10.1038/s42004-023-00841-5. ARTN 48.

[51] T. Raschle, S. Hiller, T.Y. Yu, A.J. Rice, T. Walz, G. Wagner, Structural and functional characterization of the integral membrane protein VDAC-1 in lipid bilayer nanodiscs, J. Am. Chem. Soc. 131 (49) (2009) 17777–17779, https://doi.org/10.1021/ja907918r.

[52] G. Tang, L. Peng, P.R. Baldwin, D.S. Mann, W. Jiang, I. Rees, S.J. Ludtke, EMAN2: an extensible image processing suite for electron microscopy, J. Struct. Biol. 157 (1) (2007) 38–46, https://doi.org/10.1016/j.jsb.2006.05.009.

[53] S.H.W. Scheres, A bayesian view on cryo-EM structure determination, J. Mol. Biol. 415 (2) (2012) 406–418, https://doi.org/10.1016/j.jmb.2011.11.010.